RSC Advances

PAPER

View Article Online
View Journal | View Issue

Cite this: *RSC Adv.*, 2019, **9**, 10414

A highly sensitive and selective fluorescent probe for quantitative detection of Al^{3+} in food, water, and living cells†

Qian Jiang,[a] Mingxin Li,[a] Jie Song,[b] Yiqin Yang,[cd] Xu Xu,[ad] Haijun Xu[ad] and Shifa Wang *[ad]

Received 18th January 2019
Accepted 20th March 2019

DOI: 10.1039/c9ra00447e

rsc.li/rsc-advances

Three novel β-pinene-based fluorescent probes **2a–2c** were designed and synthesized for the selective detection of Al^{3+}. Probe **2a** showed higher fluorescence intensity toward Al^{3+} than the other two compounds. Probe **2a** determined the concentration of Al^{3+} with a rapid response time (45 s), wide pH range (pH = 1–9), excellent sensitivity (LOD = 8.1×10^{-8} M) and good selectivity. The recognition mechanism of probe **2a** toward Al^{3+} was confirmed by ^{1}H NMR, HRMS and DFT analysis. Probe **2a** was successfully used as a signal tool to quantitatively detect Al^{3+} in food samples and environmental water samples. Furthermore, probe **2a** was successfully utilized to label intracellular Al^{3+}, indicating its promising applications in living cells.

1. Introduction

As the third most abundant element and the most widely used metal ion on Earth, aluminum is extensively used in a variety of fields, but is harmful to the environment and living systems.[1–4] The increasing concentration of Al^{3+} in pollutants can deeply influence the growth of plants, and lead to soil acidification[5,6] and underground water contamination.[7] Moreover, the accumulation of Al^{3+} in the body can greatly affect the absorption of calcium in bone tissue and induce several diseases such as Alzheimer's, Parkinson's epilepsy, seizures, and renal and liver damage.[8–11] In 1989, the World Health Organization (WHO) and the United Nations Food and Agriculture Organization (UNFAO) identified Al^{3+} as a food pollutant to be controlled. In 2011, WHO/UNFAO revised the weekly allowable intake of Al^{3+} from 7 mg kg^{-1} to 2 mg kg^{-1}.[12] Therefore, it is significant to detect and control the Al^{3+} concentration in water and food samples.

Compared to traditional detection methods, a fluorescent probe has become one of the most widely used tools for detecting metal ions.[13–15] In the past few years, many fluorescent probes for Al^{3+} detection have been reported.[16–25] However, there are still some shortcomings in reported Al^{3+} fluorescent probes, including a complex synthesis process, poor selectivity and sensitivity, easy interference by other metal ions, Zn^{2+}, Cu^{2+}, Cr^{3+}, Hg^{2+}, and even F^-,[26–30] and lack of applicability to water samples and food samples.[31–35] Therefore, developing a fluorescence probe with high sensitivity, good selectivity, rapid response and low toxicity for detecting Al^{3+} is particularly meaningful.

Nopinone is obtained by the oxidation of β-pinene, which is a primary ingredient in natural turpentine. It is often used in the production of medicine and perfume. In addition, the rigid structure of the nopinone molecule can reduce the energy loss of non-radiative transitions in the fluorescence emission process. Furthermore, molecules with a nopinone skeleton structure have good biological compatibility and low cytotoxicity.[36] Thus, the development of novel fluorescence probes from nopinone is very promising.

In this paper, we synthesized three new indazole derivatives for the specific detection of Al^{3+}, using natural nopinone as the starting material. Probes **2a–2c** could be synthesized by a simple two-step reaction and displayed a rapid ratiometric fluorescence toward Al^{3+} in aqueous solution (pH = 7.4). In addition, probe **2a** had a high selectivity for Al^{3+} over other metal ions and a rapid response time. The detection limit of probe **2a** was found to be 8.1×10^{-8} M, which is lower than that of many reported Al^{3+} fluorescence probes. The ^{1}H NMR, HRMS and theoretical calculations showed the detection mechanism. Furthermore, probe **2a** was successfully proved for the quantitative detection of Al^{3+} in food and environmental water samples. More importantly, cell experiments also demonstrated that probe **2a** could be used as a signal tool to detect the concentration of Al^{3+} in living cells.

2. Experimental

2.1. General information

All reagents and solvents were of analytical grade and bought from commercial sources. UV-Vis absorption spectra were

[a]*Nanjing Forestry University, China*
[b]*Department of Chemistry and Biochemistry, University of Michigan-Flint, USA*
[c]*Nanjing Forestry University, College of Chemical Engineering, China*
[d]*Institute of Chemical Engineering, Nanjing Forestry University, China*

† Electronic supplementary information (ESI) available. See DOI: 10.1039/c9ra00447e

recorded by a PerkinElmer Lambda 950. PL emission spectra were tested using PerkinElmer LS55. The ^{1}H NMR and ^{13}C NMR spectra were recorded in $CDCl_3$ solutions on a Bruker AV 400 spectrometer. The purity of the synthesized compounds was recorded by America Agilent 1260 Infinity liquid chromatography. All pH measurements were recorded using a Sartorius Basic pH-Meter PB-20. High-resolution mass spectra (HRMS) were tested by an America Agilent 5975c mass spectrometer. Melting points were recorded using an X-6 microscopic melting point apparatus. All measurements were performed at room temperature. The 5.0×10^{-5} M solutions of various metal ions (Ag^+, Hg^{2+}, Na^+, Mg^{2+}, K^+, Ca^{2+}, Fe^{2+}, Fe^{3+}, Co^{2+}, Ni^{2+}, Cu^{2+}, Zn^{2+}, Ba^{2+}, Sn^{2+}, Pb^{2+}, Cr^{2+}, Pb^{2+}, Bi^{3+} and Al^{3+}) were prepared in deionized water from their nitrate, chloride or sulfate, and stored at room temperature.

2.2. Synthesis

2.2.1. Synthesis of compounds 1a–1c. Under nitrogen atmosphere, nopinone (2 mol) was aroylated with **a–c** (3 mol) catalyzed by NaH (6 mol) in 1,2-dimethoxyethane. After cooling to room temperature, 20 ml of distilled water was added to the reaction mixture, and it was extracted with ethyl acetate. The ethyl acetate phase was washed with distilled water to neutrality. After recovering the solvent, the obtained crude **1a** was purified by column chromatography (100–200 mesh silica gel, eluent: PE : EA = 10 : 1, v/v) to obtain compounds **1a–1c**.

Compound **1a** was a pale yellow grease, yield: 71.3%; ^{1}H NMR (400 MHz, $CDCl_3$) δ: 15.58 (s, 1H), 8.68 (dd, J = 4.9, 1.7 Hz, 1H), 8.00 (d, J = 8.0 Hz, 1H), 7.88–7.72 (m, 1H), 7.35–7.30 (m, 1H), 3.28–2.95 (m, 2H), 2.59 (dt, J = 22.5, 5.4 Hz, 2H), 2.32 (qt, J = 5.9, 2.6 Hz, 1H), 1.49 (d, J = 9.9 Hz, 1H), 1.35 (s, 3H), 0.96 (s, 3H); ^{13}C NMR (100 MHz, DMSO) δ: 153.35, 148.51, 137.18, 127.72, 124.90, 123.41, 121.44, 105.43, 57.40, 54.31, 48.29, 28.34, 27.26, 25.41, 21.18; HRMS (m/z): $[M + H]^+$ calculated for $C_{15}H_{17}NO_2 + H^+$, 244.1341; found, 244.1335.

Compound **1b** was a pale yellow grease, yield: 73.8%; ^{1}H NMR (400 MHz, $CDCl_3$) δ: 15.41 (s, 1H), 8.95 (dd, J = 2.2, 0.9 Hz, 1H), 8.67 (dd, J = 4.9, 1.7 Hz, 1H), 8.03 (dt, J = 8.0, 2.0 Hz, 1H), 7.40 (ddd, J = 7.9, 4.8, 0.9 Hz, 1H), 2.71 (dd, J = 4.0, 3.0 Hz, 2H), 2.65–2.53 (m, 2H), 2.32 (tt, J = 5.9, 3.1 Hz, 1H), 1.47 (d, J = 9.5 Hz, 1H), 1.36 (s, 3H), 0.97 (s, 3H); ^{13}C NMR (100 MHz, $CDCl_3$) δ: 209.55, 169.51, 150.69, 149.01, 135.67, 131.29, 123.24, 104.89, 54.84, 39.77, 39.61, 28.07, 27.66, 25.79, 21.54; HRMS (m/z): $[M + H]^+$ calculated for $C_{15}H_{17}NO_2 + H^+$, 244.1338; found, 244.1331.

Compound **1c** was a pale yellow grease, yield: 76.5%; ^{1}H NMR (400 MHz, $CDCl_3$) δ: 15.26 (s, 1H), 8.78–8.67 (m, 2H), 7.63–7.52 (m, 2H), 2.77–2.64 (m, 2H), 2.68–2.54 (m, 2H), 2.32 (tt, J = 6.0, 3.1 Hz, 1H), 1.47 (d, J = 9.8 Hz, 1H), 1.36 (s, 3H), 0.97 (s, 3H); ^{13}C NMR (100 MHz, $CDCl_3$) δ: 209.98, 168.74, 150.06, 142.47, 122.14, 105.30, 54.92, 39.65, 39.62, 27.95, 27.60, 25.78, 21.55; HRMS (m/z): $[M + H]^+$ calculated for $C_{15}H_{17}NO_2 + H^+$, 244.1339; found, 244.1332.

2.2.2. Synthesis of 2a–2c. **1a–1c** (0.5 mmol), 60% $N_2H_4 \cdot H_2O$ (1 mmol), and 10 ml of absolute ethanol were added into a round-bottom flask equipped with a thermometer and reflux condenser. The cyclization reaction was carried out at reflux for 4 h. After recovering the ethanol, the obtained crude **2a–2c** was purified by column chromatography (100–200 mesh silica gel, eluent: PE : EA = 15 : 1, v/v) to obtain compounds **2a–2c**.

Compound **2a** was a white solid powder, yield: 85.6%, mp: 146.2–147.2 °C; ^{1}H NMR (400 MHz, DMSO) δ: 12.59 (s, 1H), 8.61 (d, J = 4.8 Hz, 1H), 7.96–7.58 (m, 2H), 7.29 (t, J = 6.3 Hz, 1H), 3.00 (dd, J = 16.3, 3.0 Hz, 1H), 2.89 (dd, J = 16.3, 2.6 Hz, 1H), 2.80 (t, J = 5.2 Hz, 1H), 2.71 (dt, J = 9.3, 5.8 Hz, 1H), 2.29 (tt, J = 5.6, 2.8 Hz, 1H), 1.39 (s, 3H), 1.27 (d, J = 9.3 Hz, 1H), 0.65 (s, 3H); ^{13}C NMR (100 MHz, $CDCl_3$) δ: 160.79, 149.58, 149.04, 137.13, 136.77, 122.19, 120.15, 110.67, 41.96, 41.30, 41.07, 32.52, 26.36, 26.32, 21.49; HRMS (m/z): $[M + H]^+$ calculated for $C_{15}H_{17}N_3 + H^+$, 240.1501; found, 240.1494.

Compound **2b** was a white solid powder, yield: 82.4%, mp: 150.5–151.5 °C; ^{1}H NMR (400 MHz, DMSO) δ: 12.61 (s, 1H), 8.94 (d, J = 2.3 Hz, 1H), 8.51 (dd, J = 4.8, 1.6 Hz, 1H), 8.07 (dt, J = 8.0, 2.0 Hz, 1H), 7.48 (dd, J = 8.0, 4.8 Hz, 1H), 2.98 (dd, J = 15.8, 3.1 Hz, 1H), 2.91–2.80 (m, 2H), 2.71 (dt, J = 9.3, 5.8 Hz, 1H), 2.31 (dt, J = 5.7, 2.9 Hz, 1H), 1.39 (s, 3H), 1.29 (d, J = 9.3 Hz, 1H), 0.66 (s, 3H); ^{13}C NMR (100 MHz, $CHCl_3$) δ: 157.91, 148.11, 146.80, 137.91, 132.80, 128.07, 123.70, 110.22, 58.08, 41.41, 41.14, 32.37, 26.23, 26.01, 21.46; HRMS (m/z): $[M + H]^+$ calculated for $C_{15}H_{17}NO_2 + H^+$, 240.1504; found, 240.1497.

Compound **2c** was a white solid powder, yield: 87.1%, mp: 157.1–158.1 °C; ^{1}H NMR (400 MHz, DMSO) δ: 12.78 (s, 1H), 8.61 (d, J = 5.1 Hz, 2H), 7.65 (d, J = 5.2 Hz, 2H), 3.00 (dd, J = 15.9, 3.1 Hz, 1H), 2.93–2.80 (m, 2H), 2.72 (dt, J = 9.4, 5.8 Hz, 1H), 2.32 (dt, J = 5.7, 2.9 Hz, 1H), 1.40 (s, 3H), 1.28 (d, J = 9.4 Hz, 1H), 0.64 (s, 3H); ^{13}C NMR (100 MHz, $CDCl_3$) δ: 157.96, 150.07, 139.12, 119.83, 111.60, 41.39, 41.33, 41.14, 32.36, 26.25, 26.21, 21.46, 18.39; HRMS (m/z): $[M + H]^+$ calculated for $C_{15}H_{17}NO_2 + H^+$, 240.1498; found, 240.1496.

2.3. Cell culture and imaging

HeLa cells were incubated with probe **2a** (5.0×10^{-6} M) in Dulbecco's Modified Eagle's Medium (DMEM) for 24 h at 37 °C. The cells were treated with aluminum chloride (5.0×10^{-5} M). After incubation for 1 h, the cells were washed with phosphate-buffered saline (PBS) three times, and the treated cells were used for cell imaging. The cell images were obtained using a confocal microscope at an excitation wavelength between 300 and 340 nm. Subsequently, in the control experiment, HeLa cells were only incubated with **2a** (5.0×10^{-6} M), and then washed with PBS three times for cell imaging. The cell images were obtained with a confocal microscope at an excitation wavelength between 300 and 340 nm.

3. Results and discussion

3.1. Synthesis and structural characteristics of probes 2a–2c

The synthetic procedure and molecular structure of probes **2a–2c** are shown in Scheme 1. The probes **2a–2c** were synthesized by two steps including the Claisen condensation of **a–c** with the β-pinene derivative nopinone catalyzed by NaH in a solution of 1,2-dimethoxyethane at reflux to obtain **1a–1c**, and **1a–1c** was further condensed with 60% $N_2H_4 \cdot H_2O$ at reflux to obtain **2a–2c**.

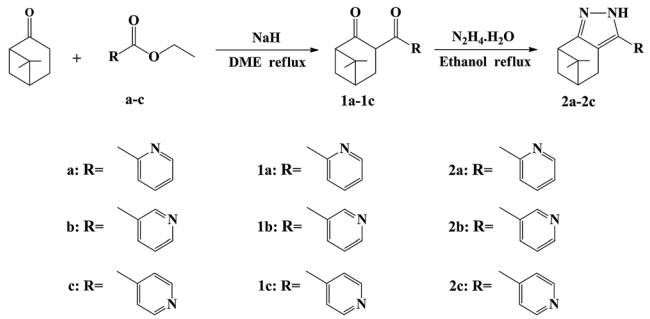

Scheme 1 Synthesis of probe 2a–2c.

3.2. Fluorescence properties of 2a–2c toward different metals

The selectivity behavior of probes **2a–2c** toward various metal ions, including K^+, Ba^{2+}, Na^+, Cr^{2+}, Co^{2+}, Mg^{2+}, Fe^{2+}, Fe^{3+}, Mn^{2+}, Ca^{2+}, Pb^{2+}, Cu^{2+}, Ag^+, Pb^{2+}, Zn^{2+}, Bi^{3+}, Ni^{2+}, Sn^{2+}, and Al^{3+} was studied by fluorescence spectroscopy. The changes in the fluorescence spectroscopy of **2a–2c** before and after the addition of various metal ions are shown in Fig. 1. This shows that compound **2a** exhibited the best selectivity and highest fluorescence intensity toward Al^{3+}, which implies a strong coordination ability between **2a** and Al^{3+}. The changes in the UV-Vis absorption spectra of **2a** before and after the addition of various metal ions are shown in Fig. S1.† Upon addition of Al^{3+} (10 equiv.) to a solution of probe **2a**, the absorption peak at 280 nm almost disappears and the peak at 330 nm is greatly enhanced. These results show that probe **2a** could be used as a fluorescent probe to selectively detect the presence of Al^{3+}.

3.3. Optimization studies of probe toward Al^{3+}

The detection conditions for probe **2a** toward Al^{3+} were optimized by investigating the influence of the concentration of **2a**, pH range, response time, and EtOH/HEPES buffer. The fluorescent intensity can reach a steady state after adding Al^{3+} into a solution of **2a** for 45 s (Fig. S2C†). Further tests for determining the selectivity and sensitivity of probe **2a** toward Al^{3+} were performed in aqueous buffer solution (EtOH/HEPES buffer, 10 mM, v/v = 6/4, pH = 7) (Fig. S2†); the concentration of probe **2a** was 5.0×10^{-6} M (Fig. S2D†). As shown in Fig. S2A,† significant enhancement in fluorescence intensity was observed in the pH range 1–9, which indicated that it is suitable for application in living systems. We studied the photo-stability of the **2a**–Al^{3+} complex in aqueous buffer solution (EtOH/HEPES buffer, 10 mM, v/v = 6/4, pH = 7). After continuous illumination for 60 h, the fluorescence intensity of the **2a**–Al^{3+} complex did not show any obvious change in fluorescence (Fig. S3†). There was good photo-stability of the **2a**–Al^{3+} complex, indicating that probe **2a** could be identified as a practical method for Al^{3+} discrimination.

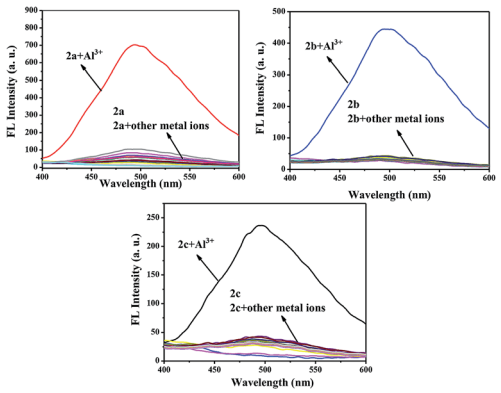

Fig. 1 Fluorescence emission spectra of **2a–2c** (5.0×10^{-6} M) upon the addition of 10 equiv. of various metal ions in C_2H_5OH solution.

3.4. Competitive selectivity of the 2a toward Al^{3+}

To further investigate the selectivity of **2a** as a fluorescence probe for Al^{3+}, competition experiments were carried out in the presence of Al^{3+} mixed with other metal ions, such as K^+, Ba^{2+}, Na^+, Cr^{2+}, Co^{2+}, Mg^{2+}, Fe^{2+}, Fe^{3+}, Mn^{2+}, Ca^{2+}, Pb^{2+}, Cu^{2+}, Ag^+, Pb^{2+}, Zn^{2+}, Bi^{3+}, Ni^{2+}, and Sn^{2+}. As shown in Fig. 2, other metal ions had very little influence on the fluorescence intensity of the **2a**–Al^{3+} complex. Combined with the data in Fig. 1, this demonstrates that probe **2a** has very high selectivity toward Al^{3+}.

3.5. Sensitivity behavior of 2a toward Al^{3+}

The sensitivity of probe **2a** toward Al^{3+} was examined with a fluorescence titration method, and the fluorescence titration spectra of probe **2a** toward Al^{3+} are shown in Fig. 3. As shown in Fig. 4B, the 5.0×10^{-6} M probe **2a** solution (EtOH/HEPES buffer, v/v = 6/4, 10 mM HEPES, pH = 7.4) exhibited non-fluorescence. Upon the addition of Al^{3+} into the probe **2a** solution (5.0×10^{-6} M), a green fluorescence dramatically appeared. Fig. 4A reveals that the fluorescence intensities at 495 nm increased linearly between the fluorescence intensity and the low Al^{3+} concentration in the range 0–1.2×10^{-5} M, $y = 63.43x + 50.82$, $R^2 = 0.9908$ (fluorescence quantum yield $\Phi = 0.49$, when the concentration of Al^{3+} was 1.5×10^{-5} M). The detection limit (LOD) for Al^{3+} was found to be 8.1×10^{-8} M by using DL = $3\sigma/k$ (where DL is the detection limit, σ is the standard deviation of the blank solution and k is the slope of the calibration plot). The association constant (K_B) of probe **2a** with Al^{3+} was determined to be 1.89×10^3 M^{-1} *via* the Benesi–Hildebrand equation[37–39] (see Fig. 4C). Table S1† summarizes the

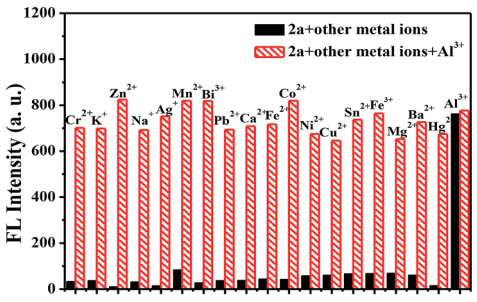

Fig. 2 Fluorescence intensity of **2a** (5.0×10^{-6} M) in buffer solution (EtOH/HEPES buffer, v/v = 6/4, 10 mM HEPES, pH = 7.4) and its complexes with Al^{3+} (5.0×10^{-5} M) in the presence of various metal ions (5.0×10^{-5} M), $\lambda_{ex} = 330$ nm.

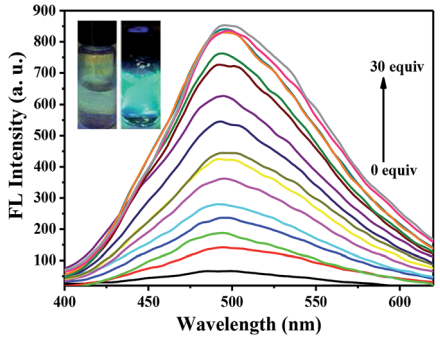

Fig. 3 Fluorescence spectral changes in **2a** (5.0×10^{-6} M) upon addition of Al^{3+} (0–1.5×10^{-5} M) in solution (EtOH/HEPES buffer, v/v = 6/4, 10 mM HEPES, pH = 7.4), λ_{ex} = 330 nm.

detection limits of recently reported Al^{3+} fluorescent sensors and highlights their applications in food samples.[40–46] The detection limit of **2a** toward Al^{3+} is the lowest among these reported probes, implying that probe **2a** can straightforwardly detect the concentration of Al^{3+} in water samples and food samples.

3.6. Binding ratio and detection mechanism between probe 2a and Al^{3+}

A Job plot experiment was carried out to determine the stoichiometry between **2a** and Al^{3+}. As shown in Fig. S4,† the stoichiometry ratio of **2a** to Al^{3+} was found to be 1 : 1. The binding mode of probe **2a** toward Al^{3+} was confirmed by ^{1}H NMR experiments in DMSO, as shown in Fig. 5. In the presence of 1.0 equiv. of Al^{3+}, the proton signal of pyrazole (H_1) disappeared and the proton signal of the pyridine moiety shifted upfield. So, the sensing mechanism of probe **2a** toward Al^{3+} could be the result of the synergistic complexation of the N atom in pyrazole and pyridine rings to Al^{3+} with a 1 : 1 stoichiometry. From the HRMS spectra (Fig. S5†), the mass peak at *m*/*z* 359.1464 corresponds to $[\mathbf{2a} + Al^{3+} + 2Cl^- + Na]^+$ (calculated at 359.2094). The proposed coordination mechanism is shown in Scheme 2. Furthermore, the energies of both the HOMO and LUMO of **2a**

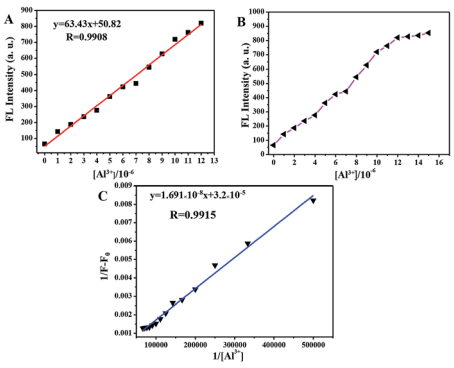

Fig. 4 (A) A linear increase in intensity at 495 nm of probe **2a** (5.0×10^{-6} M) with increasing concentrations of Al^{3+} from 0 to 1.2×10^{-5} M, λ_{ex} = 330 nm. (B) A plot of the fluorescence intensity *versus* the concentrations of Al^{3+} (0 to 1.5×10^{-5} M) in buffer solution (EtOH/HEPES buffer, v/v = 6/4, pH = 7.4). (C) Benesi–Hildebrand analysis of the emission changes for the complexation between **2a** and Al^{3+}.

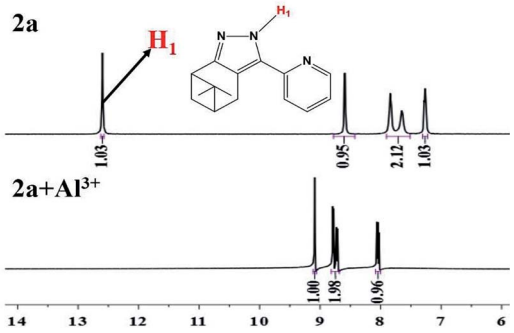

Fig. 5 ^{1}H NMR spectra changes in **2a** with the addition of Al^{3+}.

and the **2a**–Al^{3+} complex were calculated (Fig. S6†). The decrement in energy band gap confirms that there are obvious intramolecular charge-transfer (ICT) phenomena in **2a**–Al^{3+} complexes. Therefore, the calculated results were in good agreement with the emission wavelengths of **2a** and **2a**–Al^{3+}.

3.7. Preparation of the test strips

As shown in Fig. S7,† the test strips showed no fluorescence under 365 nm UV-lamp when they were prepared by soaking filter papers in an ethanol solution of **2a** (2.0×10^{-4} M) and dried in air. When immersed in an aqueous solution of Al^{3+} (2.0×10^{-4} M), the test strips showed green fluorescence. Therefore, the **2a**-based test strips show promising application for the detection of Al^{3+} in water by fluorimetric changes.

3.8. Determination in different water samples

Novel probe **2a** (5×10^{-5} M) was used for the detection of the concentration of Al^{3+} in tap water, distilled water, and lake water samples. All the water samples were collected and simply filtered. As shown in Fig. S8,† a good linear relationship was obtained between the fluorescence intensity at 495 nm and the concentration of Al^{3+} (0, 2, 5, 10, 15 $\times 10^{-6}$ M) in various water samples. The results listed in Table 1 show that in all the water samples recovery was higher than 95%. Therefore, the novel Al^{3+} fluorescent probe can be used for detection of the concentration of Al^{3+} in real water samples.

3.9. Application in food samples

It is well known that Al^{3+} is widely used in food products. But, excessive ingested Al^{3+} may cause several diseases. Therefore, it is practically important to detect Al^{3+} in food products using this novel fluorescent probe. Some food samples containing Al^{3+}, such as chips, fried chicken, tea, sausage, biscuit and baby biscuit were chosen to examine the application of probe **2a** (5×10^{-5} M) in food samples. These food samples were first crushed and 20% (v/v) HCl aqueous solution was added. Then it was stirred for one day until the solution became turbid. The mixture was filtered to obtain the Al^{3+}-containing filtrate. The fluorescence intensity at 495 nm displayed a good linear relationship with the concentration of Al^{3+} (0, 2, 5, 10, 15 $\times 10^{-6}$ M) (R^2 = 0.992, Fig. S9†). The results listed in Table 2 show that probe **2a** can detect the concentration of Al^{3+} in different food

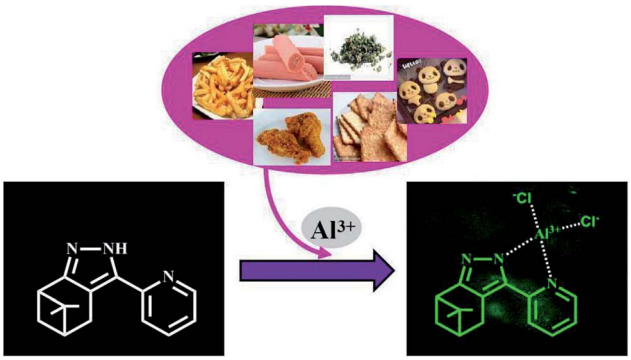

Scheme 2 Proposed coordination mechanism of **2a** with Al^{3+}.

Table 1 Application of **2a** in the determination of Al^{3+} in various water samples

Samples	Add (1×10^{-6} M)	Detected (1×10^{-6} M)	Recovery (%)
Tap water	0	0.62	0
	2	2.04	102.80
	5	5.15	103.20
	10	9.85	98.46
	15	14.93	99.54
Distilled water	0	0.17	0.00
	2	1.95	97.50
	5	5.11	102.20
	10	10.13	101.30
	15	14.69	97.96
Lake water	0	0.65	0.00
	2	1.92	96
	5	4.91	98.2
	10	10.06	100.64
	15	14.31	95.4

solutions with good recovery, ranging from 96 to 103%. Therefore, the novel Al^{3+} probe **2a** can be applied as a simple method to detect the concentration of Al^{3+} in various food samples.

3.10. Cellular imaging

Fluorescence imaging experiments of **2a** were performed to study the utility of probe **2a** in living cells. Cytotoxicity assays

Table 2 Results for the determination of Al^{3+} in various food samples

Samples	Al^{3+} (1×10^{-6} M)	Added (1×10^{-6} M)	Found (1×10^{-6} M)	Recovery (%)
Chips	6.15	3	8.99	98.25
		6	12.22	100.57
Fried chicken	5.13	3	8.32	102.33
		6	10.96	98.47
Sausage	2.89	3	5.78	98.13
		6	8.57	96.40
Tea	1.47	3	4.29	95.97
		6	7.18	96.12
Biscuit	0.55	3	3.49	98.30
		6	6.33	96.64
Baby biscuit	0	3	3.11	103.67
		6	6.12	102

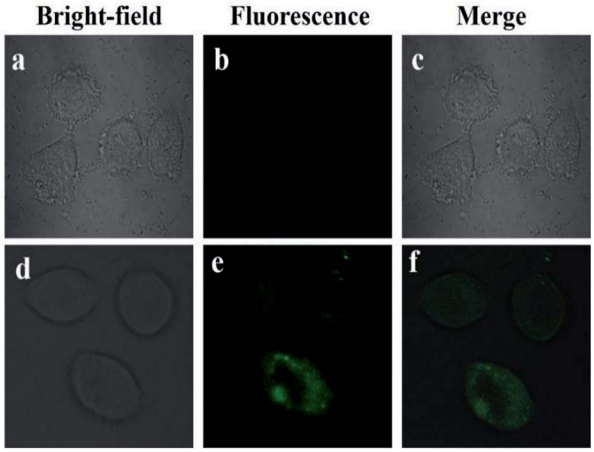

Fig. 6 (a) Fluorescent image of HeLa cells treated with probe **2a** (5.0×10^{-6} M) in the absence of Al^{3+}; (b) microscope image of HeLa cells treated with probe **2a** (5.0×10^{-6} M) in the absence of Al^{3+}; (c) merged image of frames (a) and (b); (d) microscope image of HeLa cells treated with Al^{3+} (5.0×10^{-5} M) and probe **2a** (5.0×10^{-6} M); (e) fluorescence image of HeLa cells treated with Al^{3+} (5.0×10^{-5} M) and probe **2a** (5.0×10^{-6} M); (f) merged image of frames (d) and (e).

results showed that compound **2a** had low cytotoxicity to HeLa cells (Fig. S10†). HeLa cells were incubated with **2a** (5.0×10^{-6} M) at 37 °C for 24 h. And no obvious fluorescence was observed. However, after HeLa cells were incubated with $AlCl_3$ for 1 h, remarkable fluorescence enhancement can clearly be detected (Fig. 6). The fluorescence imaging experiments show that the novel Al^{3+} fluorescent probe **2a** has potential application in living cells.

4. Conclusions

In summary, we developed a β-pinene-based fluorescent probe **2a** from natural β-pinene derivative nopinone for the detection of Al^{3+}. The new fluorescent probe **2a** exhibits advantages, such as clearer change in fluorescence, wider pH range, higher sensitivity, better selectivity, lower detection limit, and simpler synthetic procedures. The sensing mechanism of **2a** with Al^{3+} was studied by ^1H NMR, HRMS, and DFT analysis. Fluorescence probe **2a** can be used as fluorescent sensing tool for the real-time detection of Al^{3+} in aqueous media, food samples, and living cells.

Conflicts of interest

There are no conflicts to declare.

Acknowledgements

The research was supported by the National Natural Science Foundation of China (No. 31470592), Jiangsu Provincial Key Lab for the Chemistry and Utilization of Agro-Forest Biomass, the open Fund of Jiangsu Key Laboratory for Biomass Energy and Material (JSBEM201702), and Priority Academic Program Development of Jiangsu Higher Education Institutions, China.

Notes and references

1 V. K. Gupta, A. K. Singh and N. Mergu, *Electrochim. Acta*, 2014, **117**, 405–412.
2 S. Sen, T. Mukherjee and B. Chattopadhyay, *Analyst*, 2012, **137**, 3975–3981.
3 W. S. Miller, L. Zhuang and J. Bottema, *Mater. Sci. Eng., A*, 2000, **280**, 37–49.
4 N. W. Baylor, W. Egan and P. Richman, *Vaccine*, 2002, **20**, S18–S23.
5 D. Maity and T. Govindaraju, *Chem. Commun.*, 2010, **46**, 4499–4501.
6 S. Sooksin, V. Promarak and S. Ittisanronnachai, *Sens. Actuators, B*, 2018, **262**, 720–732.
7 J. L. Yang, L. Zhang and L. I. Ying, *Ann. Bot.*, 2006, **97**, 579–584.
8 J. Lee, H. Kim and S. Kim, *Dyes Pigm.*, 2013, **96**, 590–594.
9 S. Kim, J. Y. Noh, K. Y. Kim and J. H. Kim, *Inorg. Chem.*, 2012, **51**, 3597–3602.
10 P. D. Darbre, *J. Inorg. Biochem.*, 2005, **99**, 1912–1919.
11 S. R. Paik, J. H. Lee and D. H. Kim, *Arch. Biochem. Biophys.*, 1997, **344**, 325–334.
12 J. Barceló and C. Poschenrieder, *Environ. Exp. Bot.*, 2002, **48**, 75–92.
13 G. X. Zhang, R. X. Ji and X. Y. Kong, *RSC Adv.*, 2019, **9**, 1147–1150.
14 Y. Li, C. Y. Liao and S. S. Huang, *RSC Adv.*, 2016, **6**, 25420–25426.
15 T. L. Cui, S. Z. Yu and Z. J. Chen, *RSC Adv.*, 2018, **8**, 12276–12281.
16 D. P. Singh, R. Dwivedi and A. K. Singh, *Sens. Actuators, B*, 2017, **238**, 128–137.
17 X. L. Yue, Z. Q. Wang and C. R. Li, *Spectrochim. Acta, Part A*, 2017, **193**, 415–421.
18 F. Wang, Y. Xu and S. O. Aderinto, *J. Photochem. Photobiol., A*, 2017, **332**, 273–282.
19 S. R. Gupta, P. Singh and B. Koch, *J. Photochem. Photobiol., A*, 2017, **348**, 246–254.
20 Y. Wang, Z. Y. Ma and D. L. Zhang, *Spectrochim. Acta, Part A*, 2018, **195**, 157–164.
21 H. Xie, Y. Wu and J. Huang, *Talanta*, 2016, **151**, 8–13.
22 J. C. Qin, X. Y. Cheng and R. Fang, *Spectrochim. Acta, Part A*, 2016, **152**, 352–357.
23 Y. Zhang, Y. Fang and N. Z. Xu, *Chin. Chem. Lett.*, 2016, **11**, 1673–1678.
24 P. G. Ding, J. H. Wang and J. Y. Cheng, *New J. Chem.*, 2015, **39**, 342–348.
25 X. Y. Li, M. M. Yu and F. L. Yang, *New J. Chem.*, 2013, **37**, 2257–2260.
26 X. Zhang, P. Sun and F. Li, *Sens. Actuators, B*, 2017, **255**, 366–373.
27 M. Tajbakhsh, G. B. Chalmardi and A. Bekhradnia, *Spectrochim. Acta, Part A*, 2018, **189**, 22–31.
28 S. Chemate and N. Sekar, *Sens. Actuators, B*, 2015, **220**, 1196–1204.
29 B. J. Pang, C. R. Li and Z. Y. Yang, *Spectrochim. Acta, Part A*, 2018, **204**, 641–647.
30 R. Lu, S. Cui and S. Li, *Tetrahedron*, 2017, **73**, 915–922.
31 Q. Diao, P. Ma and L. Lv, *Sens. Actuators, B*, 2016, **229**, 138–144.
32 C. Lim, H. Seo and J. H. Choi, *J. Photochem. Photobiol., A*, 2018, **356**, 312–320.
33 C. Sun, J. Sun and F. Z. Qiu, *Spectrochim. Acta, Part A*, 2018, **188**, 1–7.
34 H. Liang, Z. Li and D. Wu, *Sens. Actuators, B*, 2018, **269**, 62–69.
35 Y. Tang, X. Kong and A. Xu, *Angew. Chem., Int. Ed.*, 2016, **55**, 3356–3359.
36 Z. l. Wang, Y. Zhang and J. Song, *Dyes Pigm.*, 2019, **161**, 172–181.
37 K. Huang, X. Jiao and C. Liu, *Dyes Pigm.*, 2017, **142**, 437–446.
38 J. M. Jung, J. H. Kang and J. Han, *Sens. Actuators, B*, 2018, **267**, 58–69.
39 Z. Y. Li, H. K. Su and K. Zhou, *Dyes Pigm.*, 2018, **149**, 921–926.
40 E. Feng, C. Fan and N. Wang, *Dyes Pigm.*, 2018, **151**, 22–27.
41 E. Feng, R. Lu and C. Fan, *Tetrahedron Lett.*, 2017, **58**, 1390–1394.
42 Q. Wang, X. Wen and Z. Fan, *J. Photochem. Photobiol., A*, 2018, **358**, 92–99.
43 D. Wang, X. Fan and S. Sun, *Sens. Actuators, B*, 2018, **264**, 304–311.
44 X. Gan, W. Li and C. Li, *Sens. Actuators, B*, 2017, **239**, 642–651.
45 Y. Wang, Z. Y. Ma and D. L. Zhang, *Spectrochim. Acta, Part A*, 2018, **195**, 157–164.
46 L. Li, H. Li and G. Liu, *J. Photochem. Photobiol., A*, 2017, **338**, 192–200.